This paper is published as part of a PCCP Themed Issue on:

Modern EPR Spectroscopy: Beyond the EPR Spectrum

Guest Editor: Daniella Goldfarb

Editorial

Modern EPR spectroscopy: beyond the EPR spectrum
Phys. Chem. Chem. Phys., 2009
DOI: 10.1039/b913085n

Perspective

Molecular nanomagnets and magnetic nanoparticles: the EMR contribution to a common approach
M. Fittipaldi, L. Sorace, A.-L. Barra, C. Sangregorio, R. Sessoli and D. Gatteschi, *Phys. Chem. Chem. Phys.*, 2009
DOI: 10.1039/b905880j

Communication

Radiofrequency polarization effects in zero-field electron paramagnetic resonance
Christopher T. Rodgers, C. J. Wedge, Stuart A. Norman, Philipp Kukura, Karen Nelson, Neville Baker, Kiminori Maeda, Kevin B. Henbest, P. J. Hore and C. R. Timmel, *Phys. Chem. Chem. Phys.*, 2009
DOI: 10.1039/b906102a

Papers

Radiofrequency polarization effects in low-field electron paramagnetic resonance
C. J. Wedge, Christopher T. Rodgers, Stuart A. Norman, Neville Baker, Kiminori Maeda, Kevin B. Henbest, C. R. Timmel and P. J. Hore, *Phys. Chem. Chem. Phys.*, 2009
DOI: 10.1039/b907915g

Three-spin correlations in double electron–electron resonance
Gunnar Jeschke, Muhammad Sajid, Miriam Schulte and Adelheid Godt, *Phys. Chem. Chem. Phys.*, 2009
DOI: 10.1039/b905724b

^{14}N HYSCORE investigation of the H-cluster of [FeFe] hydrogenase: evidence for a nitrogen in the dithiol bridge
Alexey Silakov, Brian Wenk, Eduard Reijerse and Wolfgang Lubitz, *Phys. Chem. Chem. Phys.*, 2009
DOI: 10.1039/b905841a

Tyrosyl radicals in proteins: a comparison of empirical and density functional calculated EPR parameters
Dimitri A. Svistunenko and Garth A. Jones, *Phys. Chem. Chem. Phys.*, 2009
DOI: 10.1039/b905522c

General and efficient simulation of pulse EPR spectra
Stefan Stoll and R. David Britt, *Phys. Chem. Chem. Phys.*, 2009
DOI: 10.1039/b907277b

Dynamic nuclear polarization coupling factors calculated from molecular dynamics simulations of a nitroxide radical in water
Deniz Sezer, M. J. Prandolini and Thomas F. Prisner, *Phys. Chem. Chem. Phys.*, 2009
DOI: 10.1039/b905709a

Dynamic nuclear polarization of water by a nitroxide radical: rigorous treatment of the electron spin saturation and comparison with experiments at 9.2 Tesla
Deniz Sezer, Marat Gafurov, M. J. Prandolini, Vasyl P. Denysenkov and Thomas F. Prisner, *Phys. Chem. Chem. Phys.*, 2009
DOI: 10.1039/b906719c

Dynamic mixing processes in spin triads of "breathing crystals" Cu(hfac)$_2$L^R: a multifrequency EPR study at 34, 122 and 244 GHz
Matvey V. Fedin, Sergey L. Veber, Galina V. Romanenko, Victor I. Ovcharenko, Renad Z. Sagdeev, Gudrun Klihm, Edward Reijerse, Wolfgang Lubitz and Elena G. Bagryanskaya, *Phys. Chem. Chem. Phys.*, 2009
DOI: 10.1039/b906007c

Nitrogen oxide reaction with six-atom silver clusters supported on LTA zeolite
Amgalanbaatar Baldansuren, Rüdiger-A. Eichel and Emil Roduner, *Phys. Chem. Chem. Phys.*, 2009
DOI: 10.1039/b903870a

Multifrequency ESR study of spin-labeled molecules in inclusion compounds with cyclodextrins
Boris Dzikovski, Dmitriy Tipikin, Vsevolod Livshits, Keith Earle and Jack Freed, *Phys. Chem. Chem. Phys.*, 2009
DOI: 10.1039/b903490k

ESR imaging in solid phase down to sub-micron resolution: methodology and applications
Aharon Blank, Ekaterina Suhovoy, Revital Halevy, Lazar Shtirberg and Wolfgang Harneit, *Phys. Chem. Chem. Phys.*, 2009
DOI: 10.1039/b905943a

Multifrequency EPR study of the mobility of nitroxides in solid-state calixarene nanocapsules
Elena G. Bagryanskaya, Dmitriy N. Polovyanenko, Matvey V. Fedin, Leonid Kulik, Alexander Schnegg, Anton Savitsky, Klaus Möbius, Anthony W. Coleman, Gennady S. Ananchenko and John A. Ripmeester, *Phys. Chem. Chem. Phys.*, 2009
DOI: 10.1039/b906827a

Ferro- and antiferromagnetic exchange coupling constants in PELDOR spectra
D. Margraf, P. Cekan, T. F. Prisner, S. Th. Sigurdsson and O. Schiemann, *Phys. Chem. Chem. Phys.*, 2009
DOI: 10.1039/b905524j

Electronic structure of the tyrosine D radical and the water-splitting complex from pulsed ENDOR spectroscopy on photosystem II single crystals
Christian Teutloff, Susanne Pudollek, Sven Keßen, Matthias Broser, Athina Zouni and Robert Bittl, *Phys. Chem. Chem. Phys.*, 2009
DOI: 10.1039/b908093g

A W-band pulsed EPR/ENDOR study of $Co^{II}S_4$ coordination in the $Co[(SPPh_2)(SP^iPr_2)N]_2$ complex
Silvia Sottini, Guinevere Mathies, Peter Gast, Dimitrios Maganas, Panayotis Kyritsis and Edgar J.J. Groenen, *Phys. Chem. Chem. Phys.*, 2009
DOI: 10.1039/b905726a

Exchangeable oxygens in the vicinity of the molybdenum center of the high-pH form of sulfite oxidase and sulfite dehydrogenase
Andrei V. Astashkin, Eric L. Klein, Dmitry Ganyushin, Kayunta Johnson-Winters, Frank Neese, Ulrike Kappler and John H. Enemark, *Phys. Chem. Chem. Phys.*, 2009
DOI: 10.1039/b907029j

Magnetic quantum tunneling: key insights from multi-dimensional high-field EPR
J. Lawrence, E.-C. Yang, D. N. Hendrickson and S. Hill, *Phys. Chem. Chem. Phys.*, 2009
DOI: 10.1039/b908460f

Spin-dynamics of the spin-correlated radical pair in photosystem I. Pulsed time-resolved EPR at high magnetic field
O. G. Poluektov, S. V. Paschenko and L. M. Utschig, *Phys. Chem. Chem. Phys.*, 2009
DOI: 10.1039/b906521k

Enantioselective binding of structural epoxide isomers by a chiral vanadyl salen complex: a pulsed EPR, cw-ENDOR and DFT investigation
Damien M. Murphy, Ian A. Fallis, Emma Carter, David J. Willock, James Landon, Sabine Van Doorslaer and Evi Vinck, *Phys. Chem. Chem. Phys.*, 2009
DOI: 10.1039/b907807j

Topology of the amphipathic helices of the colicin A pore-forming domain in *E. coli* lipid membranes studied by pulse EPR
Sabine Böhme, Pulagam V. L. Padmavathi, Julia Holterhues, Fatiha Ouchni, Johann P. Klare and Heinz-Jürgen Steinhoff, *Phys. Chem. Chem. Phys.*, 2009
DOI: 10.1039/b907117m

Structural characterization of a highly active superoxide-dismutase mimic
Vimalkumar Balasubramanian, Maria Ezhevskaya, Hans Moons, Markus Neuburger, Carol Cristescu, Sabine Van Doorslaer and Cornelia Palivan, *Phys. Chem. Chem. Phys.*, 2009
DOI: 10.1039/b905593b

Structure of the oxygen-evolving complex of photosystem II: information on the S_2 state through quantum chemical calculation of its magnetic properties
Dimitrios A. Pantazis, Maylis Orio, Taras Petrenko, Samir Zein, Wolfgang Lubitz, Johannes Messinger and Frank Neese, *Phys. Chem. Chem. Phys.*, 2009
DOI: 10.1039/b907038a

Population transfer for signal enhancement in pulsed EPR experiments on half integer high spin systems
Ilia Kaminker, Alexey Potapov, Akiva Feintuch, Shimon Vega and Daniella Goldfarb, *Phys. Chem. Chem. Phys.*, 2009
DOI: 10.1039/b906177k

The reduced [2Fe-2S] clusters in adrenodoxin and *Arthrospira platensis* ferredoxin share spin density with protein nitrogens, probed using 2D ESEEM
Sergei A. Dikanov, Rimma I. Samoilova, Reinhard Kappl, Antony R. Crofts and Jürgen Hüttermann, *Phys. Chem. Chem. Phys.*, 2009
DOI: 10.1039/b904597j

Frequency domain Fourier transform THz-EPR on single molecule magnets using coherent synchrotron radiation
Alexander Schnegg, Jan Behrends, Klaus Lips, Robert Bittl and Karsten Holldack, *Phys. Chem. Chem. Phys.*, 2009
DOI: 10.1039/b905745e

PELDOR study of conformations of double-spin-labeled single- and double-stranded DNA with non-nucleotide inserts
Nikita A. Kuznetsov, Alexandr D. Milov, Vladimir V. Koval, Rimma I. Samoilova, Yuri A. Grishin, Dmitry G. Knorre, Yuri D. Tsvetkov, Olga S. Fedorova and Sergei A. Dzuba, *Phys. Chem. Chem. Phys.*, 2009
DOI: 10.1039/b904873a

Site-specific dynamic nuclear polarization of hydration water as a generally applicable approach to monitor protein aggregation
Anna Pavlova, Evan R. McCarney, Dylan W. Peterson, Frederick W. Dahlquist, John Lew and Songi Han, *Phys. Chem. Chem. Phys.*, 2009
DOI: 10.1039/b906101k

Structural information from orientationally selective DEER spectroscopy
J. E. Lovett, A. M. Bowen, C. R. Timmel, M. W. Jones, J. R. Dilworth, D. Caprotti, S. G. Bell, L. L. Wong and J. Harmer, *Phys. Chem. Chem. Phys.*, 2009
DOI: 10.1039/b907010a

Structure and bonding of $[V^{IV}O(acac)_2]$ on the surface of AlF_3 as studied by pulsed electron nuclear double resonance and hyperfine sublevel correlation spectroscopy
Vijayasarathi Nagarajan, Barbara Müller, Oksana Storcheva, Klaus Köhler and Andreas Pöppl, *Phys. Chem. Chem. Phys.*, 2009
DOI: 10.1039/b903826b

Local variations in defect polarization and covalent bonding in ferroelectric Cu2+-doped PZT and KNN functional ceramics at themorphotropic phase boundary
Rüdiger-A. Eichel, Ebru Erünal, Michael D. Drahus, Donald M. Smyth, Johan van Tol, Jérôme Acker, Hans Kungl and Michael J. Hoffmann, *Phys. Chem. Chem. Phys.*, 2009
DOI: 10.1039/b905642d

Frequency domain Fourier transform THz-EPR on single molecule magnets using coherent synchrotron radiation

Alexander Schnegg,*[a] Jan Behrends,[a] Klaus Lips,[a] Robert Bittl[b] and Karsten Holldack[c]

Received 23rd March 2009, Accepted 1st June 2009
First published as an Advance Article on the web 23rd June 2009
DOI: 10.1039/b905745e

Frequency domain Fourier transform THz electron paramagnetic resonance (FD-FT THz-EPR) based on coherent synchrotron radiation (CSR) is presented as a novel tool to ascertain very large zero field splittings in transition metal ion complexes. A description of the FD-FT THz-EPR at the BESSY II storage ring providing CSR in a frequency range from 5 cm^{-1} up to 40 cm^{-1} at external magnetic fields from −10 T to +10 T is given together with first measurements on the single molecule magnet $Mn_{12}Ac$ where we studied $\Delta M_S = \pm 1$ spin transition energies as a function of the external magnetic field and temperature.

Introduction

Extensive EPR studies on transition metal ions (TMIs),[1,2] providing key information indispensable for a deeper understanding of their outstanding properties, proved EPR to be the method of choice to study this important class of compounds. By measuring the spin transition energies of unpaired d- or f-sub-shell electron spins exposed to the crystal field and/or an external magnetic field, EPR allows one to probe the half occupied orbitals and their delocalization onto the ligands. Interest in the magnetic properties of TMIs increased considerably when the phenomenon of single molecule magnetism was discovered in polynuclear high spin TMI complexes.[3] It was shown that single molecule magnets (SMMs) may be magnetized in an external magnetic field and stay magnetized even after switching off the magnetic field. The preconditions for this phenomenon to occur are large spin ground states, a large negative zero-field splitting (ZFS) lifting the degeneracy of the spin states at zero magnetic field, and small mixing between the spin states. These properties may lead to an energy barrier to thermal inversion of the magnetic moment at temperatures lower than the energy barrier. Concerted efforts have been undertaken to investigate and control the phenomenon of single molecule magnetism towards making it persistent even at room temperatures, which requires techniques to precisely determine the ZFSs and spin states of these compounds. However, standard EPR techniques frequently fail to detect spin transitions in high-spin systems in cases where the ZFS exceeds the quantum energy of the EPR spectrometer (typically $E_{EPR} < hc\,4\ cm^{-1}$). This problem may only be surmounted by the design and construction of novel high-frequency (and/or high-frequency/high-field) EPR spectrometers. To go beyond the limitations of standard EPR spectrometers we constructed a novel frequency domain-Fourier transform (FD-FT) THz-EPR spectrometer employing coherent synchrotron radiation (CSR) from an electron storage ring (BESSY II). Here we present first CSR based FD-FT THz-EPR measurements on the exchange coupled high spin TMI complex $Mn_{12}O_{12}(CH_3COO)_{16}(H_2O)_4]$ ($Mn_{12}Ac$),[4] the *archetypical* system for SMMs.

[a] *Helmholtz-Zentrum Berlin für Materialien und Energie, Institut für Silizium-Photovoltaik, Kekuléstr. 5, D-12489 Berlin, Germany. E-mail: alexander.schnegg@helmholtz-berlin.de; Fax: +49 (0)30 80621333; Tel: +49 (0)30 80621373*
[b] *Freie Universität Berlin, Institut für Experimentalphysik, Arnimallee 14, D-14195 Berlin, Germany*
[c] *Helmholtz-Zentrum Berlin für Materialien und Energie, Institut für Methoden und Instrumente der Synchrotronstrahlung, Albert-Einstein-Str. 15, D-12489 Berlin, Germany*

Spin Hamiltonian

The energy levels of a TMI cluster containing i unpaired electron spins without first-order orbital angular momentum exposed to an external magnetic field may be expressed by the following general spin Hamiltonian:[5,6]

$$\hat{\mathbf{H}} = \mu_B \sum_i \hat{\mathbf{S}}_i \cdot \mathbf{g}_i \cdot \hat{\mathbf{B}}_0 + \sum_{i>j} J_{ij} \hat{\mathbf{S}}_i \cdot \hat{\mathbf{S}}_j + \sum_i \hat{\mathbf{S}}_i \cdot \mathbf{D}_i \cdot \hat{\mathbf{S}}_i \quad (1)$$

Here, the first and second term are the Zeeman interaction, which couples the electron spin to the external magnetic field $\mathbf{B}_0$, and the isotropic Heisenberg exchange coupling between the electron spins $\mathbf{S}_i$ and $\mathbf{S}_j$ with coupling constant J_{ij}, respectively. The third term is the ZFS term parameterized by the ZFS tensor $\mathbf{D}$. The latter contributes only in systems with $S > 1/2$ and lifts the degeneracy of the $2S + 1$ sublevels even in the absence of an external magnetic field. It was shown that ZFS results from two contributions:[7,8] (a) the direct spin–spin coupling, originating from the dipole–dipole interactions of open-shell electron spins (to first order in perturbation theory) and (b) the spin–orbit coupling.[7]

In $Mn_{12}Ac$ the spin transition energies are determined by a magnetic core comprising a ring of eight Mn^{III} ions ($S = 2$), which are antiferromagnetically coupled to an internal tetrahedron of four Mn^{IV} ions ($S = 3/2$) (see Fig. 1). This coupling scheme leads to a total spin of $S = 10$.[3,5] The spin Hamiltonian of $Mn_{12}Ac$ is dominated by Heisenberg exchange. Therefore, the resulting spin levels may be grouped

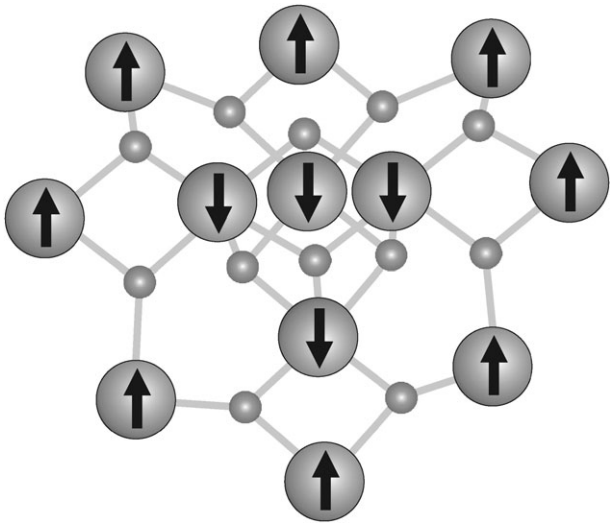

Fig. 1 Spin structure of the Mn_{12} core of $Mn_{12}Ac$ comprising eight Mn^{III} (spin up) antiferromagnetically coupled to an internal tetrahedron of four Mn^{IV} ions (spin down), giving rise to a $S = 10$ state.[3,5] Oxygen ions are depicted as gray spheres interconnecting the Mn ions.

into multiplets, each with a well defined value of S, the quantum number associated with the total spin:

$$\hat{\mathbf{S}}_{\text{tot}} = \sum \hat{\mathbf{S}}_i \tag{2}$$

In the presence of ZFS, however, the $2S + 1$ degeneracy of the multiplets is removed in a way that can be described by a spin Hamiltonian acting within each multiplet. In such an effective Hamiltonian, the ZFS and **g** tensors in eqn (1) have to be replaced by the following expressions (6):

$$\mathbf{g}_S = \sum c_i \mathbf{g}_i \tag{3}$$

$$\mathbf{D}_S = \sum d_i \mathbf{D}_i \tag{4}$$

$\mathbf{g}_i$, $\mathbf{D}_i$, the single ion **g** and ZFS tensors of the respective spin centre, contribute to the effective $\mathbf{g}_S$ and $\mathbf{D}_S$ according to the spin projection parameters c_i and d_i. The latter depend on S and S_i and may be calculated through recursive relations (6). This leads to the effective spin Hamiltonian of the total spin:

$$\hat{\mathbf{H}} = \mu_B \hat{\mathbf{S}}_{\text{tot}} \cdot \mathbf{g}_S \cdot \hat{\mathbf{B}}_0 + \hat{\mathbf{S}}_{\text{tot}} \cdot \mathbf{D}_S \cdot \hat{\mathbf{S}}_{\text{tot}} \tag{5}$$

The effective ZFS may be expanded in a series of magnetic multipoles[2] like its single ion equivalents. Recent studies have shown that in order to precisely determine the energy levels of $Mn_{12}Ac$, ZFS parameters up to the fourth order have to be taken into account.[5] These considerations are summarized in the following Hamiltonian[5] of the effective ZFS:

$$\begin{aligned}\hat{\mathbf{H}}_{\text{ZFS}} = {} & D[\hat{\mathbf{S}}_Z^2 - S(S+1)/3] \\ & + B_4^0 \hat{\mathbf{O}}_4^0 + E(\hat{\mathbf{S}}_X^2 - \hat{\mathbf{S}}_Y^2) + B_4^4 \hat{\mathbf{O}}_4^4\end{aligned} \tag{6}$$

Here D and B_4^0 are the axial and E, and B_4^4 the transverse ZFS parameters, respectively. $\mathbf{O}_m$ are Stevens operators of m-th order, which are functions of $S_{x,y,z}$.[1]

Methods

Coherent synchrotron radiation for FD-FT THz-EPR

To cover the entire energy range at which EPR transitions of TMIs may occur, instruments providing excitation frequencies ranging from a few GHz up to THz are mandatory. In zero-field EPR the spectrum can be detected by frequency sweep EPR.[9] In this mode, the spectrum is ideally detected with a single frequency scan demanding broad-band sweepable radiation sources. Due to the lack of appropriate sources, frequency domain magnetic resonance (FDMR) above 100 GHz (3.3 cm^{-1}) is usually realized by using series of backward wave oscillators.[10]

Alternatively, broader frequency scans with increased detection sensitivity may be obtained with FD-FT techniques. Exploiting the multiplex or Fellgett benefit, FT spectroscopy provides a sensitivity gain of $M^{1/2}$ against sweep techniques, where M is the number of spectral elements. However, the construction of optimized FD-FT THz-EPR instruments is limited to date by a lack of high-power broad band sources. Despite the success of FTIR studies in TMI's ZFSs[11,12] at frequencies above 1 THz, low temperature and/or high field FTIR experiments performed at lower frequencies frequently suffer from the limited power provided by standard far infra red sources. Recent studies demonstrated the possibility of synchrotron-based FT EPR experiments,[13–15] in which the authors exploited incoherent THz radiation emitted by the national synchrotron light source (NSLS, Brookhaven, USA). The potential of FD-FT THz-EPR experiments strongly increased when it was shown that ps electron bunches in electron storage rings and free electron lasers (FELs) can emit CSR up to THz frequencies,[16] providing power levels up to six orders of magnitude higher than those obtainable with incoherent synchrotron radiation.[16] Scientists at BESSY succeeded in implementing a novel electron optical mode (low α mode),[17] optimized for the generation of intense but stable THz pulses emitting broad band high power radiation in the frequency range from 5 cm^{-1} to 40 cm^{-1} (150 GHz to 1.2 THz, see Fig. 1). Based on these advances in accelerator technology we succeeded in setting up a FD-FT THz-EPR spectrometer at the dedicated THz beamline in section H11 of the BESSY II storage ring (see Fig. 2). Here CSR is coupled out of the storage ring by a low-loss quasioptical THz transmission line[18] through a z-cut quartz window serving as radiation outlet on top of the storage ring. The THz beam propagating in (vacuum) free space is then focused on the external radiation port of a FTIR-spectrometer (optional Bruker™ Vertex 70, min. bandwidth: 0.5 cm^{-1}) by off-axis parabolic mirrors. Highly sensitive detection is obtained by liquid helium-cooled InSb and Si bolometers as well as by pyroelectric crystal based detectors (deuterated triglycin sulfate). In order to exploit the maximum frequency range accessible with unimpaired stability we employed narrow band lock-in-detection (Perkin-Elmer 7280) for the InSb detector locked to the repetition frequency (1.25 MHz) of the electron macro pulses (see inset in Fig. 2). Thereby the steady state CSR component may be demodulated from additional low frequency amplitude modulations caused by bursting CSR at

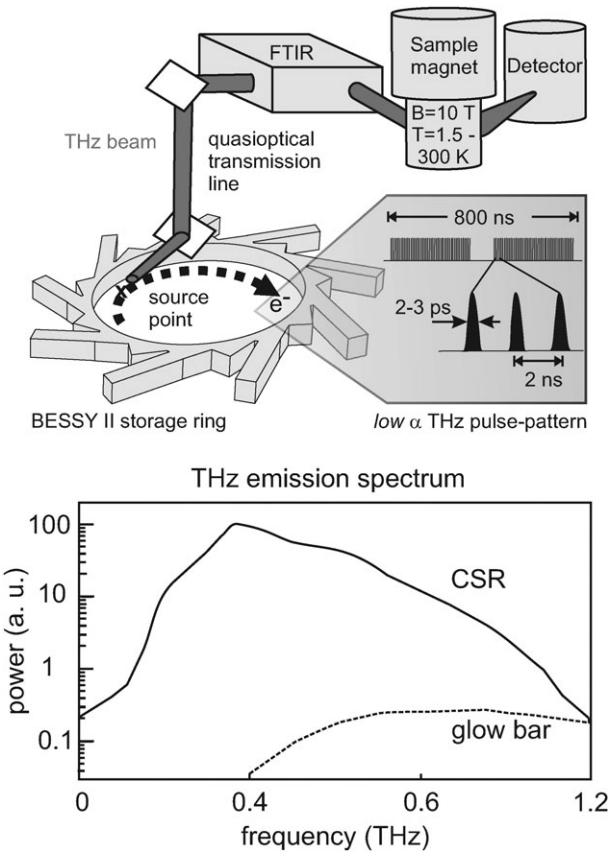

Fig. 2 (Top) Scheme of the quasioptical FD-FT THz-EPR set-up consisting of the radiation extraction optics in the storage ring, the quasioptical THz transmission line, the FTIR spectrometer, the superconducting magnet with variable temperature insert (Oxford Spectromag 4000, $B_0 = \pm 10$ T, $T = 1.5$–300 K), and the detector. The THz pulse pattern from the electron bunches in the storage ring are depicted in the box with a gray background. Depending on the fill pattern of the storage ring in the low α mode, in general 350 2-to-3 ps long micro pulses with a time spacing of 2 ns form a macro pulse arriving with a 1.25 MHz repetition rate. (Bottom) FT detected THz emission spectra of the BESSY storage ring driven in low α mode at a ring current of 30 mA (solid) and the glow bar source of the FTIR spectrometer (dashed). Both spectra were detected under identical conditions. The spectral shape of the FT detected CSR is determined by the electron bunch length and charge, the beam diameter of the quasioptical transmission line (causing a cut-off at 150 GHz) as well as the beamsplitter in the FTIR spectrometer. With increasing ring current the electron bunches become asymmetric and experience instabilities. Both effects extend the emission spectrum to higher wave numbers at increasing ring current.

high current levels. This extends the usable current range to values of twice the instability threshold. The detection technique presented here paves the way for even broader frequency scans at higher power levels, which are achievable by higher ring currents. This type of demodulation techniques may make FD-FT THz-EPR accessible to other storage rings not being able to shorten the bunches by a lower momentum compaction, but employing CSR from instabilities instead. Variation of the sample temperature and the magnetic field at the sample position was obtained by inserting a liquid helium-cooled cryostat (Oxford Optistat, $T = 1.5$–300 K) or alternatively a super conducting magnet with a variable temperature insert (Oxford Spectromag 4000; $B_0 = \pm 10$ T, $T = 1.5$–300 K), both equipped with THz transparent windows, into the beam path. The magnet is equipped with four *z*-cut quartz windows, which allows for orienting the magnetic field parallel or perpendicular to the linearly polarized light from the storage ring. In order to correct for the frequency dependent emission spectrum of the electron bunches and to discriminate electric dipole transitions in the air and in the sample material from spin induced magnetic dipole transitions, the FT spectra taken at very low temperature were divided by reference spectra taken at thermal energies well above the energy of the ground state spin transitions. Thereby, ground state spin transitions may be recorded as absorption changes originating from temperature dependent population changes of the spin levels. The described detection scheme allowed us to detect a minimum number of spins of $\sim 10^{18}$ ($Mn_{12}Ac$, $S = 10$).

Results and discussion

Zero-field/high-frequency EPR

Fig. 3 displays FD-FT THz-EPR spectra of $Mn_{12}Ac$ taken at $T = 4.5$ K, 10 K and 15 K. Depending on the sample temperature, one, two or three EPR lines can be identified in the absorption spectra (see dotted lines in Fig. 3). At 4.5 K, the EPR spectrum is dominated by a strong absorption line at 10 cm^{-1} (300 GHz). Upon increasing the temperature to 15 K the intensity of this line decreases and vanishes above 40 K (data not shown). Above 4.5 K two additional absorption lines are identified at 8.3 cm^{-1} (250 GHz) and 6.9 cm^{-1} (210 GHz) with pronounced temperature dependence. The relative intensity of the line at 8.3 cm^{-1} as compared to the line at 10 cm^{-1}

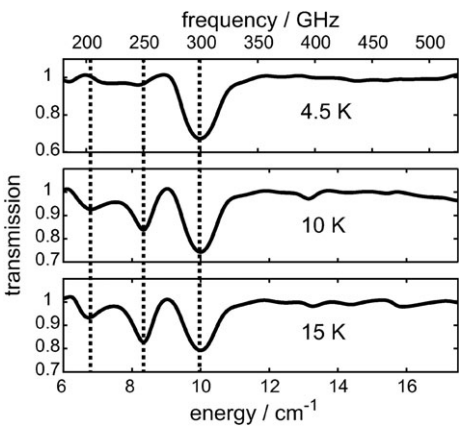

Fig. 3 FD-FT THz-EPR spectra of $Mn_{12}Ac$ obtained at $T = 4.5$ K, 10 K and 15 K. The spectra were obtained by dividing the spectra through a reference spectrum taken at 50 K. In the EPR spectra absorption lines resulting from $\Delta M_S = \pm 1$ EPR transitions are indicated by dotted lines. From left to right these are the $M_S = \pm 8$ to $M_S = \pm 7$ (6.9 cm^{-1}), the $M_S = \pm 9$ to $M_S = \pm 8$ (8.3 cm^{-1}) and $M_S = \pm 10$ to $M_S = \pm 9$ (10 cm^{-1}) transitions, respectively. Experimental conditions: sample amount: 50 mg, THz source: synchrotron in low α mode, averaged cw-power $P_{THz} = 5$ mW, detector: LHe cooled InSb-bolometer, spectral resolution: 0.5 cm^{-1}, data acquisition time per spectrum: 5 min.

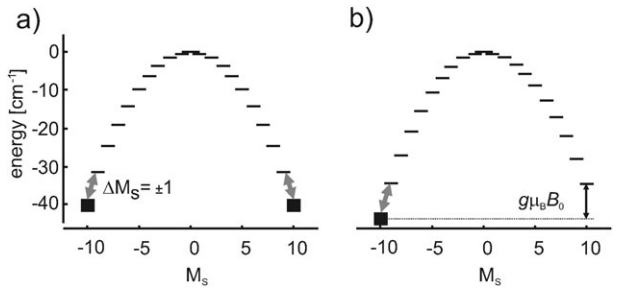

Fig. 4 Energies of the M_S spin levels belonging to the ground manifold $S = 10$ (a) at zero magnetic field and (b) with an applied external magnetic field B_0. At zero magnetic field and low temperatures (hc 10 cm^{-1} $\approx$ k 14.5 K) only the energetically lowest-lying energy levels $M_S = \pm 10$ are populated (■). Therefore, only the $\Delta M_S = \pm 1$ transitions (grey arrows) may be observed in the EPR spectrum (see Fig. 3 and 5). At sufficiently high temperatures also the higher lying M_S states are populated and spin transitions $\Delta M_S = \pm 1$ transitions among these states may be observed (see Fig. 3). An external magnetic field B_0 lifts the degeneracy of the ground states levels and shifts their transition energies (see Fig. 5). Relaxation induced by the magnetic field $B_0 > 0$ ($B_0 < 0$) shifts the spin population to the $M_S = -10$ ($M_S = +10$) state.

clearly increases with increasing temperature until their intensities equalize at about 15 K. The spectral position of the three lines, as well as the temperature dependence of their relative intensities, may be rationalized by the magnetic properties of $Mn_{12}Ac$. In $Mn_{12}Ac$ negative ZFS lifts the $S = 10$ spin ground state's degeneracy leading to an energy barrier Δ towards thermal inversion of the magnetic moment. The height of the barrier $\Delta = k$ 61 K is determined by the axial terms of the ZFS tensor and the effectiveness of phonon activated quantum tunneling processes.[19] The ZFS parameters for $Mn_{12}Ac$ have been determined to high accuracy by FDMRS,[20] inelastic neutron scattering (INS)[21] and high field EPR.[22] Due to resolution restrictions in our current set-up we are not able to improve the accuracy of the ZFS parameters extracted from the literature, however recent instrument upgrades showed that the accuracy of FD-FT THz-EPR may be significantly improved by employing an ultra high resolution FTIR spectrometer. Inserting the axial ZFS parameters into eqn (6) the spin transition energies may be calculated and the observed absorption lines assigned to the following M_S ($S = 10$) transitions (see Fig. 4). At temperatures below the energy of the $M_S = \pm 10$ to $M_S = \pm 9$ ground state transition at 10 cm^{-1} (hc 10 cm^{-1} $\approx$ k 14.5 K), only the lowest lying energy states are populated (see Fig. 4). Upon rising the temperature, the energetically higher lying $M_S = \pm 9$ and $M_S = \pm 8$ become populated leading to additional absorption lines at 8.3 cm^{-1} ($M_S = \pm 9$ to $M_S = \pm 8$) and 6.9 cm^{-1} ($M_S = \pm 8$ to $M_S = \pm 7$). When increasing the temperature above 40 K the absorption lines in the FD-FT THz-EPR spectra of $Mn_{12}Ac$ vanish since their intensities are too small to be distinguished from the noise floor. At these temperatures even lower lying energy transitions should be populated, which cannot be observed with the described setup due to a low frequency cut-off at 5 cm^{-1} (150 GHz). Recording FD-FT THz-EPR at zero magnetic field ZFS parameters may be determined avoiding field dependent line broadening mechanisms resulting from the anisotropy of the magnetic interaction tensors (see eqn (1)). Zero field FD-EPR on the other hand clearly suffers from the fact that FD THz spectroscopy is sensitive to both magnetic as well as electric dipole transitions. This leads to an overlap of absorption lines resulting from spin transition and soft vibrational modes in the FD-FT spectrum. Elimination of this ambiguity may be obtained by the employment of strong external magnetic fields shifting magnetic transitions but leaving electric dipole transitions unchanged.

High-field/high-frequency EPR

Fig. 5 depicts FD-FT THz-EPR detected transmission spectra of the first mode ($M_S = \pm 10$ to $M_S = \pm 9$) of $Mn_{12}Ac$ ($T = 4.5$ K) at varying external magnetic fields. We found that, when increasing the external magnetic field, the centre of the resonance position shifts to higher transition energies in addition to a strong field dependent line broadening. Due to the line broadening the resonance line cannot be distinguished from the noise floor at magnetic fields above 4 T (data not shown). From an inspection of the spin Hamiltonian (eqn (5)) it becomes apparent that the line shifts may be attributed to the field dependent Zeeman interaction.

Fig. 4 shows an energy scheme of the M_S spin levels belonging to the $S = 10$ ground state at zero magnetic field (a) and with an applied external magnetic field B_0 (b) along the "easy axis" of the magnetic anisotropy.[19] The Zeeman interaction splits the resonance lines in the EPR spectrum symmetrically in two components centred about the zero field position. However, in order to fully rationalize the field-dependent line shape changes, the powder character of the sample as well as field induced population changes of the spin levels have to be taken into account. In the present case we studied randomly oriented $Mn_{12}Ac$ molecules exposed to linearly polarized electromagnetic radiation with a field vector

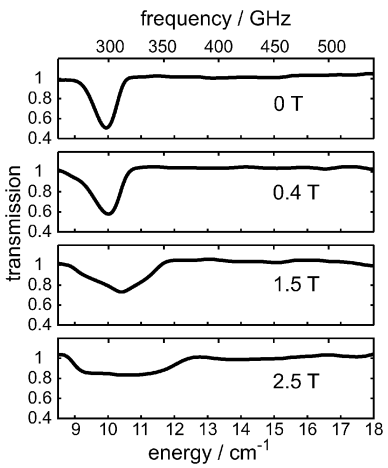

Fig. 5 FD-FT THz-EPR spectra of $Mn_{12}Ac$ obtained at $T = 4.5$ K and at external magnetic fields $B_0 = 0$ T, 0.4 T, 1.5 T and 2.5 T. The spectra were obtained by dividing the spectra through a reference spectrum taken at 50 K. Experimental conditions: sample amount: 50 mg, THz Source: synchrotron in low α mode, averaged cw-power $P_{THz} = 5$ mW, detector: LHe cooled InSb-bolometer, spectral resolution: 0.5 cm^{-1}, data acquisition time per spectrum: 5 min.

perpendicular to the external magnetic field. In this case different molecules in the sample experience different external magnetic fields depending on the relative orientation of the molecules' "easy axis" with respect to the external magnetic field, which causes inhomogeneous field dependent broadening of the EPR resonance lines. This broadening mechanism can be avoided by studying single crystals,[10] which in addition provides information about the orientation of the ZFS tensor with respect to the molecular axis system. Additional asymmetry of the line shape is introduced by field-induced population changes of the energetically lowest lying energy states. An increase of the external magnetic field to $B_0 > 0$ ($B_0 < 0$) leads to metastabilty of the $M_S = -10$ ($M_S = +10$) states.[10] This leads to fast relaxation to the lowest lying energy states, resulting in increased line intensities in the FD-FT THz-EPR spectrum at the energetically higher-lying resonances at expenses of their lower-lying counterparts.[10] The possibility to monitor field induced intensity changes on the time scale of minutes is of particular interest when studying quantum tunnelling phenomena in SMMs.[19]

Conclusion and outlook

The obtained results demonstrate the possibility to assign the absolute value of SMMs' energy-barrier-determining ZFS by rapid scan FD-FT THz-EPR. Due to the broad excitation spectrum of CSR, single scan spectra ranging from 5 cm^{-1} up to 40 cm^{-1} at different external magnetic fields may be obtained on the time scale of minutes. Such studies are not restricted to SMMs but may easily extended to other mono- or multinuclear TMI complexes. The information content extractable from FD-FT THz-EPR can be further increased by employing high-resolution FT spectroscopy to determine ZFS parameters with improved accuracy. In order to exploit this benefit we recently included an ultra high resolution FTIR spectrometer (Bruker IFS 125HR) in our set-up. The improved set-up will allow for frequency scans with a resolution of 0.006 cm^{-1} ($\sim$200 MHz), which is comparable to BWO based frequency domain magnetic resonance spectrometers, but still beyond the resolution of single frequency high-field EPR spectrometers (resolution typically $<$10 MHz). In the case of SMMs, where recent studies demonstrated that a resolution of a few hundred MHz is sufficient to resolve the shape of the EPR spectrum, the inferior resolution of FD-FT THz-EPR and FDMR techniques is usually more than compensated by the access to a very broad range of transition frequencies. The main advantages of FD-FT THz-EPR over FDMR approaches lies in its potentially higher sensitivity due to the Multiplex benefit and the possibility to scan the resonance frequency over a very broad range with a single source. Further differences between sweep techniques like single frequency EPR and FDMR on the one hand and FD-FT THz-EPR on the other arise from the fact that, for the latter, the entire spectrum is excited at once. This is of particular importance while studying spin relaxation phenomena below or close to the blocking temperature where spin relaxation processes on the time scale of the spectrum acquisition time may alter the relative intensities in the spectrum during the sweep. The short data acquisition time of FD-FT THz-EPR as compared to complementary techniques like INS allows detailed temperature scans yielding important information about the temperature dependence of the spin populations and pave the way for studies in magnetic field induced quantum tunnelling phenomena and spin phonon couplings with improved resolution and sensitivity as compared to INS.[23] It is worthwhile noting here that EPR and INS are sensitive to spin transitions with different selection rules (EPR: $\Delta M_S = \pm 1$, $\Delta S = \pm 0$ and INS: $\Delta M_S = 0, \pm 1, \Delta S = 0, \pm 1$) yielding complementary information on the spin systems. Further on, FD-FT THz-EPR spectroscopy may be the method of choice for accurate measurements on complex spin systems, sensitive samples with impurities, and particularly also on solutions, for which magnetic susceptibility data suffer severely from the diamagnetic contribution of the solvent.

Acknowledgements

The authors gratefully acknowledge helpful discussions with M. Fuchs (Paul Scherrer Institute), J. van Slageren (The University of Nottingham), E. Bill (Max-Planck-Institut für Bioanorganische Chemie) and B. Lake (Helmholtz-Zentrum Berlin für Materialien und Energie) and JvS for kindly providing the $Mn_{12}Ac$ sample. In addition we would like to thank D. Ponwitz and T. Seefeldt for skilful technical assistance and the BESSY accelerator group for setting up the low-α mode. This work was generously supported by the German Federal Ministry of Education and Research (BMBF, network project EPR-Solar/03SF0328A/C/E).

References

1 A. Abragam and B. Bleaney, *Electron Paramagnetic Resonance of Transition Ions*, Dover Publications, Inc., New York, 1986.
2 J. R. Pilbrow, *Transition Ion Electron Paramagnetic Resonance*, Clarendon Press, Oxford, 1990.
3 A. Caneschi, D. Gatteschi, R. Sessoli, A. L. Barra, L. C. Brunel and M. Guillot, *J. Am. Chem. Soc.*, 1991, **113**, 5873–5874.
4 T. Lis, *Acta Crystallogr., Sect. B: Struct. Crystallogr. Cryst. Chem.*, 1980, **36**, 2042–2046.
5 D. Gatteschi, A. L. Barra, A. Caneschi, A. Cornia, R. Sessoli and L. Sorace, *Coord. Chem. Rev.*, 2006, **250**, 1514–1529.
6 A. Bencini and D. Gatteschi, *EPR of Exchange Coupled Systems*, Springer Verlag, Berlin, 1990.
7 F. Neese, in *Calculation of NMR and EPR Parameters. Theory and Applications*, ed. M. Kaupp, M. Bühl and V. G. Malkin, Wiley-VCH, Weinheim, 2004, pp. 541–566.
8 R. Boca, *Coord. Chem. Rev.*, 2003, **248**, 757–815.
9 R. R. Joyce and P. L. Richards, *Phys. Rev.*, 1969, **179**, 375.
10 J. van Slageren, S. Vongtragool, B. Gorshunov, A. A. Mukhin, N. Karl, J. Krzystek, J. Telser, A. Müller, C. Sangregorio, D. Gatteschi and M. Dressel, *Phys. Chem. Chem. Phys.*, 2003, **5**, 3837.
11 P. J. Van der Put and A. A. Schilperoord, *Inorg. Chem.*, 1974, **13**, 2476–2481.
12 K. Ray, A. Begum, T. Weyhermuller, S. Piligkos, J. van Slageren, F. Neese and K. Wieghardt, *J. Am. Chem. Soc.*, 2005, **127**, 4403–4415.
13 L. Mihály, D. Talbayev, L. F. Kiss, J. Zhou, T. Fehér and A. Jánossy, *Phys. Rev. B: Condens. Matter Mater. Phys.*, 2004, **69**, 024414.
14 D. Talbayev, L. Mihaly and J. Zhou, *Phys. Rev. Lett.*, 2004, **93**, 017202.
15 S. d. Brion, C. Darie, M. Holzapfel, D. Talbayev and L. Mihaly, *Phys. Rev. B: Condens. Matter Mater. Phys.*, 2007, **75**, 094402.

16 G. L. Carr, M. C. Martin, W. R. McKinney, K. Jordan, G. R. Neil and G. P. Williams, *Nature*, 2002, **420**, 153.
17 M. Abo-Bakr, J. Feikes, K. Holldack, P. Kuske, W. B. Peatman, U. Schade, G. Wüstefeld and H. W. Hübers, *Phys. Rev. Lett.*, 2003, **90**, 094801.
18 K. Holldack and D. Ponwitz, *AIP Conf. Proc.*, Daegu, Korea, 2007.
19 D. Gatteschi and R. Sessoli, *Angew. Chem., Int. Ed.*, 2003, **42**, 268.
20 A. A. Mukhin, V. D. Travkin, A. K. Zvezdin, S. P. Lebedev, A. Caneschi and D. Gatteschi, *Europhys. Lett.*, 1998, **44**, 778–782.
21 I. Mirebeau, M. Hennion, H. Casalta, H. Andres, H. U. Gudel, A. V. Irodova and A. Caneschi, *Phys. Rev. Lett.*, 1999, **83**, 628–631.
22 A. L. Barra, D. Gatteschi and R. Sessoli, *Phys. Rev. B: Condens. Matter Mater. Phys.*, 1997, **56**, 8192.
23 O. Waldmann, G. Carver, C. Dobe, D. Biner, A. Sieber, H. U. Gudel, H. Mutka, J. Ollivier and N. E. Chakov, *Appl. Phys. Lett.*, 2006, **88**, 042507.